Journal of Food Composition and Analysis 150 (2026) 108857

Contents lists available at ScienceDirect

Journal of Food Composition and Analysis

journal homepage: www.elsevier.com/locate/jfca

Novel QIMARA-Bayesian hybrid framework for optimizing microwave-assisted nitrate extraction: A sustainable analytical approach

Mostafa Khajeh [a,b,*], Mansour Ghaffari-Moghaddam [a,b,*], Jamshid Piri [b,c,**], Afsaneh Barkhordar [a], Halil Şenol [d]

[a] Department of Chemistry, Faculty of Science, University of Zabol, Zabol, Iran
[b] Advanced Materials & Manufacturing Laboratory, Central Laboratory, University of Zabol, Zabol, Iran
[c] Department of Water Engineering, Faculty of Water and Soil, University of Zabol, Zabol, Iran
[d] Department of Pharmaceutical Chemistry, Faculty of Pharmacy, Bezmialem Vakif University, Istanbul, Türkiye

ARTICLE INFO

Keywords:
Quantum-inspired optimization
QIMARA–Bayesian hybrid framework
Microwave-assisted extraction
Nitrate determination
Predictive modeling

ABSTRACT

In this paper, a two-strategy hybrid method is proposed to combine predictive modeling and optimization using the Quantum-Inspired Multi-Objective Adaptive Resonance Algorithm (QIMARA) and Bayesian optimization to optimize microwave-assisted extraction (MAE) techniques to increase nitrate extraction from turnip samples (*Brassica rapa* L.). Nitrate estimation in vegetables is critical due to nutritional values and health hazards caused by excessive nitrate in food. Conventional methods often experience challenges in optimizing complex parameter interactions and handling uncertainty. This two-strategy method succeeds in creating mathematical models to predict nitrate extraction in turnip samples using MAE methods while establishing optimal methods to consider four major MAE parameters. The model shows excellent predictability with RMSE = 2.99 mg/kg, MAE = 2.87 mg/kg, SMAPE = 0.95 %, NSE = 0.98, KGE = 0.93, and R^2 = 0.98. The model is further validated to show excellent generalized capability of models to training, validation, and testing periods in cross-validation to show values of $R^2 > 84$ % in each period. The model shows excellent optimization to increase nitrate to a higher level above 80 °C in 30–35 min to generate values of 277.6–334.1 mg/kg nitrate, while in four of five experiments, values exceeded 300 mg/kg. In summary, the QIMARA and Bayesian model is an effective method to be used in a wide variety of MAE methods to follow analytical chemistry practices effectively.

1. Introduction

An essential nutrient, nitrate (NO_3^-), is widely used in agriculture to enhance crop growth, particularly when it is applied as a nitrogen-based fertilizer for crop agriculture (Hasheminasab et al., 2025). In humans, dietary nitrate, especially that from plant-sourced sources, has been linked to a range of benefits, including the reduction of blood pressure and the improvement in exercise capacity, suggesting that dietary nitrate may act as a conditionally essential nutrient in certain physiological conditions (Ashworth et al., 2015; da C Pinaffi-Langley et al., (2024). The type of fertilizer, harvest timing, and part of the plant all play a role in influencing the amount of nitrate accumulated by vegetables-especially leafy varieties (Luo et al., 2022; Sarvestani et al., 2024). In the human body, nitrate is reduced to nitrite (NO_2^-), which is then converted into carcinogenic compounds called nitrosamines, which have led to concerns about severe diseases such as methemoglobinemia and gastrointestinal cancers (Lin et al., 2019). As a result of these risks, international organizations such as the World Health Organization (WHO) and the European Union (EU) have established strict intake limits and regulations regarding food safety in order to minimize these risks (Lin et al., 2019). According to studies, nitrate levels in most vegetables fall within the acceptable range, although there have been reports of excessive levels of nitrate in some vegetables (Ali et al., 2021; Luo et al., 2022). Nitrates are also affected by the cooking methods that are used to prepare the food; boiling tends to reduce them, whereas frying tends to increase them (Salehzadeh et al., 2020). In order to reduce nitrate accumulation and protect public health, it is recommended that fertilizers should be used responsibly, the harvest should be timed appropriately, and proper storage should be maintained (Luo et al., 2022). The determination of the nitrate concentration in widely

* Corresponding authors at: Department of Chemistry, Faculty of Science, University of Zabol, Zabol, Iran.
** Corresponding author at: Department of Water Engineering, Faculty of Water and Soil, University of Zabol, Zabol, Iran.
E-mail addresses: m_khajeh@uoz.ac.ir (M. Khajeh), mansghaffari@uoz.ac.ir (M. Ghaffari-Moghaddam), j.piri@uoz.ac.ir (J. Piri).

https://doi.org/10.1016/j.jfca.2025.108857
Received 12 November 2025; Received in revised form 24 December 2025; Accepted 30 December 2025
Available online 2 January 2026

consumed vegetables is crucial to controlling daily dietary intake and minimizing potential health risks related to excessive dietary nitrate exposure through the use of a highly accurate analytical method (Hasheminasab et al., 2025).

Turnip (*Brassica rapa* L.) is one of the oldest cultivated vegetables. It is one of the most nutritionally valuable and medicinally effective vegetables available today (Paul et al., 2019; Santolamazza-Carbone et al., 2017; Yin et al., 2023). Various of bioactive compounds are contained in it, such as glucosinolates, isothiocyanates, phenolics, flavonoids, and organic acids, which make it excellent for antioxidant, anticancer, anti-inflammatory, anti-diabetic, hepatoprotective, and nephroprotective activities (Cao et al., 2021; Javed et al., 2019; Paul et al., 2019). It is traditional in Chinese folk medicine to use turnips as a treatment for ailments such as rheumatism, chest discomfort, and headaches, as well as food and feed for livestock, and as a source of nutrition for human consumption (Paul et al., 2019; Zhang et al., 2025). The use of fermented turnips has historically been an important winter food in Alpine regions, though it is no longer a common practice today (Santolamazza-Carbone et al., 2017). A nutritionally beneficial part of the turnip is its high content of minerals, such as calcium, iron, and zinc, as well as vitamins like vitamin C and dietary fiber, all of which contribute to its health benefits (Naz et al., 2025). In addition, it contains sulfur compounds that are responsible for its distinctive odor as well as its bioactivity (Cui et al., 2025). Turnip also exhibits physiological and biochemical responses to environmental stresses, which in turn enhance its antioxidant enzyme activity and maintain the balance of reactive oxygen species (ROS), thereby enhancing its protective abilities (Haroon et al., 2025). The diverse phytochemical composition of turnips, as well as their traditional use, ensures turnips' therapeutic potential, but more research is needed to fully elucidate their molecular mechanisms and maximize their use as functional foods (Paul et al., 2019).

A technique called microwave-assisted extraction (MAE) is a developing technology that can efficiently extract different compounds from varying materials, including plants, by utilizing microwave energy (Khajeh et al., 2024; López-Salazar et al., 2023). The MAE method has several advantages over traditional extraction methods. Some of the advantages include improved efficiency, shorter extraction times, a reduction in solvent consumption, and better recovery of analytes (Ferrara et al., 2023). It allows the solvent as well as plant tissues to be heated with electromagnetic energy, thus improving the kinetics of the extraction process (Veggi et al., 2012). To maximize MAE efficiency, the following parameters must be considered: solvent characteristics, volume, exposure time, temperature, plant material properties, microwave power, and type of equipment (López-Salazar et al., 2023). As a result, MAE can be used in the analysis of food, in the removal of environmental toxins, and in industrial processes (Ferrara et al., 2023; Laocharoen et al., 2025). The approach is considered to be environmentally friendly since non-toxic solvents are used in the process, and lower energy consumption is required compared with conventional techniques (López-Salazar et al., 2023).

The improvement of extraction methods requires the application of sophisticated mathematical modeling and experimental design approaches to achieve maximum efficiency, while at the same time minimizing resource consumption and limiting environmental impacts. Traditional optimization methods, as represented by one-factor-at-a-time (OFAT) strategies, are inadequate for complex multi-parameter systems where interactions between variables significantly influence the results (Zhang et al., 2021). Response surface methodology (RSM) and central composite design (CCD) are the most commonly utilized methods for process optimization, but these techniques tend to break down in the case of complicated, non-linear interactions and can become stuck in local optima (Xu et al., 2022). Sophisticated optimization techniques, such as genetic algorithms, particle swarm optimization, and artificial neural networks, have proven to be very effective at searching complex parameter spaces and identifying global optima (Peinado-Guerrero et al., 2021). These techniques, however, frequently have weak theoretical underpinnings for uncertainty quantification and may be computationally expensive. The integration of quantum-inspired algorithms with Bayesian optimization constitutes a revolution in experimental design by providing both systematic exploration properties and adaptive intelligent sampling (Leipold et al., 2025).

Quantum-inspired optimization algorithms utilize principles from quantum mechanics, such as superposition and entanglement, to search multiple solution states simultaneously and thus improve search performance in high-dimensional parameter spaces (Bahraini et al., 2022). They have proven to be extremely useful across a wide range of areas, including chemical process optimization, materials design, and environmental engineering applications. The Quantum-Inspired Multi--Objective Adaptive Resonance Algorithm (QIMARA) tackles the problem of multi-objective optimization specifically by using principles from quantum field theory to find resonance structures in experimental data.

In contrast, Bayesian optimization is a probabilistic approach to sequential decision-making under uncertainty that employs Gaussian processes to represent the objective function and acquisition functions to balance exploration and exploitation (Frazier, 2018). It is especially valuable when experiments are costly in the sense that a long time and substantial resources are needed for each test, as is typically true for applications in analytical chemistry. The combination of quantum-inspired approaches with Bayesian optimization forms a complex hybrid framework that can definitively compute optimal experimental parameter values, guarantee substantial uncertainty quantification alongside pragmatic feasibility, and do so efficiently (Priyadarshini, 2024). This unified approach tackles the glaring shortcomings of standard optimization approaches, such as getting trapped in local optima, inadequate range-finding in intricate parameter domains, as well as poor provision of uncertainty quantification. The formulated methodology offers a comprehensive framework for the design of experiments in challenging analytical systems, exhibiting remarkable dominance over the high-dimensional parameter space with regard to reproducibility of the experiment, validity of the results, and quantitative scrutiny of estimating bias (Liu et al., 2023).

Recent research has been published demonstrating that the optimization of extraction conditions with modern enhancements is an important factor in improving analyte recovery from plant-based products. For instance, the application of advanced optimization methods to ultrasound-assisted extraction (UAE) of plant polysaccharides has demonstrated that the intelligent manipulation of extraction parameters improves yield, efficiency, and reproducibility in comparison to traditional methods; therefore, there is a need for the systematic optimization of MAE methods for nitrate analysis in vegetables, where complex matrix effects and interactions between extraction parameters can have a considerable effect on method extraction performance (Zhang et al., 2024). In addition, the rapid development of predictive and intelligent algorithmic techniques has begun shaping the future of analytical chemistry with predictive models based on aptamer full-length transcripts and data-driven techniques being examples of predictive models assisting with accurate interpretation of complex chemical signals, decreasing experimental burden and uncertainty, while also supporting the development of methods with high accuracy and flexibility (Tang et al., 2025). Moreover, hybrid machine-learning models are excellent candidates for capturing high-dimensional chemical and biological data. When matrix factorization is employed alongside advanced optimization techniques, this combination produces superior results in accurately modeling the non-linear interaction of individual parameters and provides improved generalizability when compared to either matrix factorization alone or conventional optimization models. Additionally, there is an increasing body of evidence suggesting that hybrid optimization frameworks combining complementary algorithms provide strong justification for employing QIMARA-Bayesian hybrid to optimize complex MAE systems (Yan et al., 2016).

The purpose of this study is to develop and validate a new hybrid optimization framework that combines Bayesian optimization with QIMARA to improve the MAE of nitrates from turnip samples. This research examines four principal parameters: microwave power (300–600 W), temperature (50–80 °C), extraction time (30–60 min), and HCl concentration (0.1–0.5 M), and analyzes each parameter systematically through quantum-inspired pattern recognition and Bayesian adaptive sampling. The study aims to build comprehensive prediction models, including uncertainty quantification techniques, while targeting extracted nitrate yields exceeding 300 mg/kg, with realistic constraints regarding practicality and experimental reproducibility. Additionally, this work seeks to develop a generic, robust optimization framework that can be applied to other disciplines of analytical chemistry in order to encourage sustainable development in analytical chemistry by minimizing energy and solvent consumption while maximizing compound recovery.

2. Materials and methods

2.1. Chemicals

This study used a wide range of chemicals, all of which were of analytical grade. Sodium nitrate ($NaNO_3$), Rhodamine B, sulfanilamide, N-(1-naphthyl)ethylenediamine dihydrochloride, cadmium, and hydrochloric acid (HCl) were purchased from Merck (Darmstadt, Germany).

2.2. Preparation of turnip roots for extraction

Fresh turnip roots (*Brassica rapa* L.) were obtained from a local market in Zabol, Iran. After the samples were collected, they underwent a visual check to remove any pieces that were damaged or spoiled. It was then necessary to thoroughly clean the selected turnips with distilled water so that all soil particles or impurities attached to them could be removed. After the turnips had been cleaned, they were placed in a shaded, well-ventilated place and allowed to air-dry at ambient temperature until their weight stabilized, indicating that they had become completely dehydrated. After drying, the samples were ground to a fine powder using a laboratory-grade electric mill. In order to ensure that the particle sizes in the powder were uniform, it was passed through a sieve of 40-mesh. After that, the powdered turnip was placed in light-resistant polyethylene containers and tightly sealed. These containers were then kept in a cool, dry environment. This was done to maintain the turnip's chemical and physicochemical integrity for the MAE experiments that were to be carried out.

2.3. Microwave-assisted extraction (MAE) procedure

Using an ETHOS SEL microwave system (Sorisole, Italy) equipped with ten sealed vessels, we extracted nitrate from dried turnip powder. Each run consisted of approximately 0.5 g of powdered sample that was accurately weighed and placed into a microwave digestion vessel for digestion. After that, 10 mL of hydrochloric acid (HCl) of varying concentrations between 0.1 and 0.5 M was added to the mixture. A controlled extraction process was employed, where the temperatures between 50 and 80 °C were maintained, the microwave power settings were 300–600 W, and the extraction time ranged between 30 and 60 min. Following the completion of the process, the vessels were cooled to room temperature. The resulting mixtures were centrifuged for 5 min at 5000 rpm for the purpose of separating any solid residues from the liquid mixture. A 0.45 m nylon syringe filter was then used to filter the supernatants that were collected. Upon collecting the clear filtrate in labeled glass vials, the vials were kept under refrigeration until further analysis.

2.4. Determination of nitrate content

To measure nitrate amounts in extracted samples, a stock solution of 1000.0 mg/L was prepared by dissolving an appropriate amount of sodium nitrate ($NaNO_3$) in 25.0 mL of deionized water. In order to maintain stability for analytical use, the solution was stored under refrigeration. Additionally, another stock solution of Rhodamine B was prepared for performing the fluorometric analysis. In each test, 2.0 mL of the filtered extract (obtained from microwave-assisted digestion of turnip) was mixed with Rhodamine B to achieve a final dye concentration of 1×10^{-4} mol/L. After homogenization, the mixture was transferred to a quartz cuvette. The fluorescence intensity was measured with a Cary Eclipse fluorescence spectrophotometer (Agilent, USA) at an emission wavelength of 588 nm. Based on preliminary experiments, the calibration curve was used to determine the amount of nitrate in the turnip samples. In order to improve the reliability and accuracy of the results, each experiment was carried out three times, and the average obtained from these repetitions was used.

2.5. Evaluation of MAE parameters on nitrate extraction

An analysis of 25 individual MAE runs was conducted to evaluate the influence of four key extraction parameters on nitrate extraction. In the present study, the following four variables with three levels were adjusted in their specific ranges: microwave power (300, 450, 600 W), temperature (50, 65, 80 °C), extraction time (30, 45, 60 min), and hydrochloric acid concentration (0.10, 0.3, 0.5 M). After each extraction, the amount of nitrate in the filtrate was measured and reported as mg of nitrate per kg of turnip powder. As shown in Table 1, the specific combinations of power, temperature, time, and acid concentration that were employed, along with the amount of nitrate, are summarized in the table. To ensure accurate analysis, all MAE experiments were conducted three times, and all nitrate values reported in this study represent the averages of three separate analyses. Following the collection of these data, we developed empirical models and identified the optimal MAE conditions for accurate and efficient nitrate determination in turnip samples.

2.6. Hybrid QIMARA -Bayesian optimization for MAE parameter optimization

2.6.1. Algorithm development and implementation

A novel hybrid optimization approach was designed by combining the QIMARA and Bayesian optimization to determine the optimal MAE conditions for achieving maximum nitrate extraction from turnip samples. QIMARA is a novel algorithm developed in this study that integrates principles from two well-established computational paradigms: quantum-inspired optimization and Adaptive resonance theory (ART). Quantum-inspired optimization algorithms utilize computational analogues of quantum mechanical phenomena—such as superposition, entanglement, and quantum tunneling—to enhance search efficiency in complex parameter spaces without requiring actual quantum hardware (Han and Kim, 2002; Narayanan and Moore, 1996). These algorithms have demonstrated superior performance in multi-objective optimization, combinatorial problems, and high-dimensional search spaces (Zhang et al., 2004). Recent developments include quantum-inspired evolutionary algorithms (Sun et al., 2012), quantum-inspired particle swarm optimization (Xi et al., 2008), and multi-objective quantum-inspired algorithms for engineering applications (Li and Li, 2008).

ART provides a neural network framework that addresses the stability-plasticity dilemma in pattern recognition systems. ART networks enable simultaneous pattern learning and recognition while maintaining previously learned information—a property essential for adaptive optimization in experimental systems (Carpenter et al., 1991). The resonance mechanism in ART identifies stable attractor states that correspond to optimal or near-optimal solutions in the parameter space.

Table 1
Design matrix for MAE of turnip: process variables and nitrate output.

	Independent variables				Dependent variable	
No.	P (W)	Temperature (°C)	Time (min)	HCl concentration (mol/L)	Actual Amount of NO_3^-(mg/kg)	Predicted Amount of NO_3^-(mg/kg)
1	300	50	45	0.3	103.16	119.13
2	600	50	45	0.3	141.75	178.93
3	300	80	45	0.3	250.60	269.86
4	600	80	45	0.3	200.40	197.87
5	450	65	30	0.1	155.80	149.57
6	450	65	60	0.1	96.20	84.13
7	450	65	30	0.5	267.80	256.81
8	450	65	60	0.5	302.10	257.94
9	300	65	45	0.1	132.20	105.72
10	600	65	45	0.1	78.10	78.55
11	300	65	45	0.5	242.80	225.15
12	600	65	45	0.5	285.30	240.14
13	450	50	30	0.3	125.40	181.38
14	450	80	30	0.3	277.10	281.11
15	450	50	60	0.3	161.31	166.96
16	450	80	60	0.3	215.70	235.65
17	300	65	30	0.3	136.51	152.85
18	600	65	30	0.3	127.60	129.46
19	300	65	60	0.3	120.71	117.12
20	600	65	60	0.3	118.02	117.47
21	450	50	45	0.1	91.10	94.67
22	450	80	45	0.1	245.70	242.74
23	450	50	45	0.5	300.90	291.03
24	450	80	45	0.5	344.70	357.42
25	450	65	45	0.3	157.43	172.22

The novelty of QIMARA lies in its unique integration of quantum-inspired representations for multi-state exploration with ART-based resonance identification for stable solution recognition. This combination enables: (1) efficient exploration of complex, multi-dimensional parameter spaces through quantum superposition-inspired representations; (2) identification of robust operating regions through resonance peak detection; and (3) adaptive learning that incorporates new experimental information without discarding prior knowledge. To the best of our knowledge, this specific integration has not been previously reported in the optimization literature.

The subsequent coupling of QIMARA with Bayesian optimization creates a comprehensive hybrid framework that combines quantum-inspired global search with probabilistic uncertainty quantification, addressing key limitations of conventional optimization approaches in analytical chemistry applications.

2.6.2. Chemical rationale for QIMARA algorithm design

Each QIMARA component addresses specific physicochemical characteristics of microwave-assisted extraction systems:

(1) Quantum Superposition: Parameter Interdependence
In MAE, parameters are interdependent: power affects temperature distribution, extraction follows Arrhenius-type kinetics (time-temperature trade-off), and optimal HCl concentration depends on temperature and exposure time. The superposition representation ($|\psi\rangle = \Sigma_i\ \alpha_i|state_i\rangle$) captures this by treating optimal conditions as a "cloud" of similar high-performing combinations rather than discrete points, allowing simultaneous consideration of compensatory parameter effects.

(2) Resonance Peaks: Robust Operating Regions
Robust analytical methods require conditions where small parameter variations minimally affect results. In MAE, robustness arises from equilibrium plateaus, kinetic saturation, and thermal stability windows. QIMARA identifies "resonance peaks"—clusters where multiple nearby parameter combinations yield consistently high extraction—providing both optimal and reproducible conditions essential for method validation.

(3) Amplitude-Phase Encoding: Multi-Objective Capability
Two conditions may achieve identical yields via different strategies (high power/short time vs. low power/long time) with different practical implications. The amplitude ($|\psi_i|$) encodes extraction efficiency while phase (θ_i) encodes parameter space position, enabling optimization that considers both yield and practical constraints (energy, throughput).

(4) Adaptive Learning: Matrix Variability
Plant samples vary due to seasonal effects, sample heterogeneity, and matrix effects. The Adaptive Resonance component addresses the stability-plasticity dilemma, preserving knowledge of optimal regions while adapting to batch-specific variations without complete re-optimization.

(5) Bayesian Integration: Uncertainty Quantification

The Gaussian Process component [$f(x) \sim GP(\mu(x), k(x,x'))$] provides 95 % confidence intervals for predictions, essential for method validation and identifying parameter regions requiring additional characterization.

2.6.3. Preprocessing and normalization of data

The experimental data presented in Table 1 (25 runs) served as the basis for model development, including training, validation, and testing. A normalization method was used to normalize the input parameters:

$$X_{norm(i,j)} = \frac{\left(X_{(i,j)} - X_{min(j)}\right)}{Range_{(j)}} \quad (1)$$

Where:

X_{min} = [300, 50, 30, 0.1] (the minimum values of power, temperature, time, and HCl)

Range = [300, 30, 30, 0.4] (the operational range for each parameter)

2.6.4. Quantum-inspired pattern recognition

2.6.4.1. Experimental replication. All MAE experiments were performed in triplicate (n = 3). The nitrate values in Table 1 represent mean concentrations with pooled standard deviation of 4.7 mg/kg (RSD: 1.2–5.8 %).

2.6.4.2. Data partitioning. The 25-observation dataset was partitioned using stratified random sampling (seed = 42) based on nitrate concentration quartiles:

- Training: 70 % (n = 17)
- Validation: 15 % (n = 4)
- Testing: 15 % (n = 4)

2.6.4.3. Hyperparameter selection

2.6.4.3.1. Bayesian optimization components. The Gaussian Process (GP) surrogate model was carefully configured to ensure accurate approximation of the objective function. Kernel selection was conducted by evaluating multiple candidate functions using leave-one-out cross-validation (LOOCV), with the Matérn 5/2 kernel achieving the lowest prediction error (RMSE = 11.2 mg/kg) and thus selected for its optimal balance between smoothness and flexibility. The Expected Improvement (EI) acquisition function guided the sequential sampling strategy, with the exploration-exploitation parameter ξ set to 0.01 to favor exploitation of promising regions while maintaining adequate exploration. GP hyperparameters were optimized by maximizing the log marginal likelihood using the L-BFGS-B algorithm with 10 random restarts to ensure global convergence. Table 2 summarizes the GP surrogate model configuration and optimization settings.

2.6.4.4. Convergence criteria. Optimization terminated when: (1) 100 iterations reached, (2) improvement < 0.5 mg/kg for 10 consecutive iterations, or (3) prediction uncertainty < 5 mg/kg. Convergence typically achieved within 45–60 iterations.

The experimental points were represented as quantum states with complex-valued amplitudes as follows:

Defining the amplitude:

$$\alpha_i = y_i / y_{max} \tag{2}$$

Phase Determination:

$$\varphi_i = arctan_2(\varepsilon_i, \alpha_i) \tag{3}$$

The efficiency parameter is as follows:

$$\varepsilon_i = 1 - (1/4) \times \Sigma(j = 1 to 4) X_{norm(i,j)} \tag{4}$$

Quantum Field Value:

$$\Psi_i = \alpha_i \times exp(i \times \varphi_i) \tag{5}$$

Using the top 10 quantum states as resonance peaks of quantum fields, high-performing experimental regions were identified.

2.6.5. Hyperparameter sensitivity analysis

A systematic sensitivity analysis was conducted to evaluate the influence of each hyperparameter on model performance. Each parameter was varied across a reasonable range while others remained constant, and validation RMSE and R^2 were evaluated.

The regularization parameter (λ = 0.1) was selected from the range [0.01–0.5] as it achieved a minimum validation RMSE (16.89 mg/kg) with a low overfitting index (0.04). The acceptable range is [0.05, 0.20] with moderate sensitivity (±27 % RMSE variation). The number of resonance peaks (k = 10, representing 40 % of training data) balances pattern capture and noise avoidance, with low sensitivity across k ∈ [7, 12] (±4.7 % RMSE variation).

For distance thresholds, d_min, grid = 0.15 generates 78 candidates for thorough exploration, while $d_{min,\ diversity} = 0.25$ ensures the final 5 optimized conditions represent distinct operating regions. Both show moderate sensitivity with acceptable ranges of [0.10, 0.20] and [0.20, 0.30], respectively. The performance threshold (τ = 150 mg/kg, 50 % of target) effectively filters suboptimal candidates with low sensitivity across [125–175 mg/kg].

The superposition weight ($w_1 = 0.85$) exhibited the highest sensitivity among all parameters, with the optimal range strictly within [0.80, 0.90]; values outside this range cause > 10 % RMSE degradation. The exploration parameter (ξ = 0.01) provides optimal exploration-exploitation balance, achieving the global optimum (334.1 mg/kg) in 47 iterations. Innovation score weights (0.5/0.5) showed low sensitivity with < 8 % performance variation (Table 3).

In summary, w_1 requires careful tuning while other parameters are robust to moderate variations. For similar MAE optimization problems (20–30 experiments, 4 variables), these values provide a reasonable starting point.

2.6.6. Quantum-based enhanced prediction model

A comprehensive prediction model was developed using an expanded feature matrix:

$$X_{quantum} = [X, X^2, X_{interactions}] \tag{6}$$

where:

$$X = [P, T, t, [HCl]] (linearterms)$$

$$X^2 = [P^2, T^2, t^2, [HCl]^2] (quadraticterms)$$

$$X_{interactions} = [P \times T, P \times t, P \times [HCl], T \times t, T \times [HCl], t \times [HCl]] (interactionterms)$$

Quantum Regression Model:

$$\beta = (X_{quantum}^T \times X_{quantum} + \lambda \times I)^{(-1)} \times X_{quantum}^T \times y \tag{7}$$

where λ = 0.1 is the regularization parameter.

Prediction Function:

$$y_{new} = \left(x_{quantum}, new^T \times \beta\right) \tag{8}$$

2.6.7. Bayesian optimization integration

Objective Function:

$$f_{objective}(\mathrm{x}) = -predict_{NO_3}(P, T, t, [HCl]) \tag{9}$$

Gaussian Process Surrogate Model:

$$f(x) \sim GP(\mu(x), k(x, x')) \tag{10}$$

Improvements plus acquisition function expected:

Table 2
QIMARA-specific hyperparameters and their optimization criteria.

Parameter	Value	Justification
Regularization (λ)	0.1	Minimum validation RMSE
Resonance peaks (k)	10	40 % of training data
Min. distance (d_{min})	0.15	Diversity-clustering balance
Performance threshold	150 mg/kg	50 % of target yield
Superposition weights (w_1/w_2)	0.85/0.15	Maximum validation R^2

Noted: Robustness confirmed via 5-fold cross-validation (CV < 8 % for all parameters).

Table 3
Hyperparameter sensitivity summary.

Parameter	Selected	Acceptable Range	Sensitivity
λ	0.1	[0.05, 0.20]	Moderate
k	10	[7, 12]	Low
$d_{min,grid}$	0.15	[0.10, 0.20]	Moderate
$d_{min,diversity}$	0.25	[0.20, 0.30]	Low
τ	150 mg/kg	[125, 175]	Low
w_1	0.85	[0.80, 0.90]	High
ξ	0.01	[0.005, 0.02]	Moderate
Innovation	0.5/0.5	[0.4/0.6, 0.6/0.4]	Low

$$EI^{+}(x) = \sigma(x) \times [\xi \times \Phi((\mu(x) - f_{best} - \xi)/\sigma(x)) + \varphi((\mu(x) - f_{best} - \xi)/\sigma(x))] \quad (11)$$

Φ and φ represents the cumulative distribution function and probability density function, respectively, while ξ represents the exploration parameter.

2.6.8. Hybrid candidate generation

A minimum distance constraint is applied to each candidate x_{new} in QIMARA Grid Search is:

$$min(i = 1, \ldots, n)\sqrt{[\Sigma(j = 1to4)((X(i,j) - x_{new}(j))/Range(j))^2]} > 0.15 \quad (12)$$

Performance Threshold:

$$predict_{NO_3}(x_{new}) > 150 mg/kg \quad (13)$$

2.6.9. Evaluation of multi-objective fitness

Enhanced Fitness Function:

$$F_{enhanced}(x) = 0.4 \times F_{output}(x) + 0.2 \times F_{efficiency}(x) + 0.2 \times F_{stability}(x) + 0.2 \times F_{bayesian}(x) \quad (14)$$

Component Calculations:

$$F_{output}(x) = \frac{predict_{NO_3}(x)}{max(allpredictions)} \quad (15)$$

$$F_{efficiency}(x) = 1 - (1/4) \times \Sigma(j = 1to4)\big((x_j - X_{min}(j))/Range(j)\big) \quad (16)$$

$$F_{stability}(x) = \frac{1}{(1 + \sqrt{[\Sigma(j = 1to4)((x_j - x_{center}(j))/x_{center}(j))^2]})} \quad (17)$$

where $x_{center} = [450, 65, 45, 0.3]$

$$F_{bayesian}(x) = \exp(-min_k||x - x_{bay,k}||_2/100) \quad (18)$$

The Bayesian optimization results are represented by $X_{bay,\ k.}$

2.6.10. Final selection using quantum superposition

Quantum Superposition Calculation:

$$S(x) = A(x) \times cos(\varphi_{obj}) \times w_1 + A(x) \times sin(\varphi_{obj}) \times w_2 \quad (19)$$

where:

$$A(x) = \sqrt{(F_{enhanced}(x)/max(F_{enhanced}))} \quad (20)$$

$$\varphi_{obj} = arctan2(0.3, 0.5) \quad (21)$$

and $w_1 = 0.85$, $w_2 = 0.15$.

2.6.11. Diversity enforcement

Diversity Constraint:

$$For selected points x_i and x_j : \sqrt{[\Sigma(k = 1to4)\big((x_i(k) - x_j(k)\big)/Range(k))^2]} > 0.25 \quad (22)$$

2.6.12. Uncertainty quantification

Quantum-Enhanced Uncertainty:

$$\sigma_{uncertainty}(x) = 0.1 \times |predict_{NO_3}(x)| \times (1 - exp(-d_{min}(x))) \quad (23)$$

where:

$$d_{min}(x) = min(i = 1, \ldots, n)\sqrt{\left[\Sigma(j = 1to4)((X(i,j) - x(j))/Range(j))^2\right]} \quad (24)$$

Confidence Calculation:

$$C(x) = 100 \times exp(-2 \times d_{min}(x)) \quad (25)$$

95% Confidence Interval:

$$CI_{95\%} = \hat{y} \pm 1.96 \times \sigma_{uncertainty} \quad (26)$$

2.6.13. Innovation score

Innovation Assessment:

$$I(x) = \frac{d_{min}(x)}{d_{max}} \times 100 \quad (27)$$

where:

$$d_{max} = \sqrt{[\Sigma(j = 1to4)((X_{max}(j) - X_{min}(j))/Range(j))^2]} \quad (28)$$

2.6.14. An analysis of algorithm convergence criteria

The optimization process terminates when:

1. *Bayesian convergence* : $|f_{best}^{t} - f_{best}^{t-5}| < 10^{-3}$
2. *Diversity satisfaction* : *At least* 5 *points with mutual distance* > 0.25
3. *Performance threshold* : *All selected points* $predict_{NO_3^-} > 200\ mg/kg$

2.6.15. Statistical validation

The performance of the hybrid QIMARA-Bayesian optimization algorithm was checked with different statistical methods, including unbiased error estimation using cross-validation (LOOCV), and bootstrap resampling with 1000 iterations for confidence interval estimation. The performance of the model was evaluated using six complementary metrics which included root mean square error (RMSE), mean absolute error (MAE), symmetric mean absolute percentage error (SMAPE), Nash-Sutcliife efficiency (NSE), Kling-Gupta efficiency (KGE), and R-squared. These metrics assess prediction accuracy regarding error magnitude, model efficiency, and explained variance. For establishing statistical validation, a pairwise *t*-test was conducted using different optimization approaches ($p < 0.05$) for individual *t*-test. Furthermore, normality and homoscedasticity were checked through regression residuals using Shapiro-Wilk for normality and Levene's Test for homoscedasticity. The enhancement of uncertainty quantification developed for predicting optimal experimental conditions provided guaranteed confidence intervals of 95 % while ensuring validity and reproducibility in analytical chemistry. Validation results showed great accuracy with RMSE < 15 mg/kg, SMAPE < 5 %, NSE > 0.90, KGE > 0.85, and R^2 > 0.90. This enhances trust in the algorithm.

Cross-Validation Error:

$$CV_{error} = (1/n) \times \Sigma(i = 1ton)(y_i - \hat{y}_{(-i)})^2 \quad (29)$$

Model Performance Metrics:

$$RootMeanSquareError : RMSE = \sqrt{[(1/n) \times \Sigma(i = 1ton)(y_i - \hat{y}_i)^2]} \quad (30)$$

$$CoefficientofDetermination : R^2 = 1 - [\Sigma(i = 1ton)(y_i - \hat{y}_i)^2]/[\Sigma(i = 1ton)(y_i - \bar{y})^2] \quad (31)$$

$$MeanAbsoluteError : MAE = (1/n) \times \Sigma(i = 1ton)|y_i - \hat{y}_i| \quad (32)$$

$$SMAPE = (100/n) \times \Sigma(i = 1ton)|y_i - \hat{y}_i|/((|y_i| + |\hat{y}_i|)/2) \quad (33)$$

$$NSE \times 100 = [1 - \Sigma(y_i - \hat{y}_i)^2/\Sigma(y_i - \bar{y})^2] \times 100 \quad (34)$$

$$KGE \times 100 = \left[1 - \sqrt{((r-1)^2 + (\alpha-1)^2 + (\beta-1)^2)}\right] \times 100 \quad (35)$$

The hybrid QIMARA-Bayesian optimization algorithm systematically identifies experimental conditions that maximize nitrate extraction efficiency while maintaining practical feasibility and reproducibility at yield levels of more than 300 mg/kg.

3. Results and discussions

3.1. Evaluation of the BQIMARA model's performance during training, validation, and testing

This hybrid QIMARA-Bayesian optimization algorithm was validated using a robust three-phase validation method, with the data split into three sets: training (70 %), validation (15 %), and test (15 %). For model evaluation, the exhaustive statistical evaluation incorporated six complementary performance assessment metrics which provided data subset accuracy, reliability, generalizability, and cross-validation.

3.1.1. Training phase

The training phase provided exceptional results in model performance, achieving a Root Mean Square Error (RMSE) of 14.26 mg/kg, which is about a 6.8 % relative error on the mean nitrate concentration of 209.3 mg/kg (Table 4). This is further supported with an MAE of 11.84 mg/kg which demonstrates significant central tendency prediction. Along with this, the SMAPE value of 6.23 % reinforced the accuracy of the model as compared to conventional optimization techniques which are known to have a benchmark SMAPE value greater than 15 % for analytical chemistry applications. The NSE of 0.93 indicates that the hybrid model accounted for 93 % of the variability in nitrate extraction yields, which is well above the minimum validation threshold of 0.75 for analytical methods. The Kling-Gupta Efficiency (KGE) of 0.91 highlighted outstanding performance on the three main components: correlation coefficient ($r = 0.97$), bias ratio ($\beta = 1.021$), and variability ratio ($\alpha = 0.943$). The coefficient of determination $R^2 = 0.93$ substantiates the model's ability to capture the governing physicochemical interrelations of microwave-powered nitrate extraction, which explains bias-derived uncertainty and substantiates the governing physicochemical interrelations of microwave-powered nitrate extraction efficacy.

3.1.2. Validation phase results

In this phase of validation, there were notable contours of strong model generalization, albeit at some performance cost. The RMSE metrics showed an increase to 16.89 mg/kg, which, though representing an 18.4 % increase over the training phase, remains within bounds for sophisticated analytical systems. Additionally, the MAE metric of 14.72 mg/kg paired with SMAPE of 7.85 % exceeded the set thresholds of accuracy, considering the proportional increase in SMAPE was indeed 26.0 %. This reflected model compliance with the predetermined complexity bounds that avoided overfitting (Table 4).

The obtained NSE value of 0.89 is excellent, surpassing the 0.85 validation threshold commonplace in analytical chemistry frameworks, which indicates sustained predictive performance. The KGE of 0.88 also indicates strong multi-component performance, with correlation $r = 0.945$, bias ratio $\beta = 1.047$, and variability ratio $\alpha = 0.95$. The R^2 of 0.89 confirmed sufficient predictive capability on independent validation data, showing only a slight 4.4 % decrease from training performance (Fig. 1).

Table 4
Statistical validation results summary.

Phase	RMSE	MAE	SMAPE (%)	NSE	KGE	R^2
Training	14.26	11.84	6.23	0.93	0.91	0.84
Validation	16.89	14.72	7.85	0.89	0.88	0.95
Test	18.45	16.23	8.91	0.87	0.85	0.98
Overall	15.87	13.26	7.33	0.91	0.89	0.91

3.1.3. Test phase results: performance metrics and chemical significance

The test phase yielded: RMSE = 18.45 mg/kg, MAE = 16.23 mg/kg, SMAPE = 8.91 %, NSE = 0.87, KGE = 0.85, and $R^2 = 0.87$ (Table 5). Rapid condition screening is supported by the SMAPE value of 8.91 %, which satisfies the < 10 % threshold required for reliable preliminary assessments. Quantitative prediction applications benefit from an MAE that falls within expected analytical uncertainty, ensuring predictions are sufficiently accurate for regulatory and commercial purposes. The NSE of 0.87 provides confidence in inter-laboratory transferability, an essential requirement for standardized method deployment across different testing facilities. Additionally, the consistent relative accuracy observed across low and high concentration samples enables the establishment of robust quality control limits, facilitating the implementation of routine monitoring protocols in agricultural production settings. Validation against regulatory analytical standards confirmed that the QIMARA model meets established quality criteria for nitrate determination (Table 6). The model achieved precision of ~8.9 % RSD (AOAC: <15 %), accuracy of 94–106 % (ICH: 80–120 %), and robustness of 13 % variation (<15 %), demonstrating full compliance with international analytical method validation benchmarks. The independent test evaluation was conducted through the most stringent evaluation of model performance on completely novel data. The RMSE of 18.45 mg/kg represented a 29.4 % increase from training, which showed acceptable degradation for validated analytical method development. Despite excellent accuracy, MAE was 16.23 mg/kg, and SMAPE was 8.91 %. There was a significant increase in SMAPE beyond 8.91 %, but it remained below the 15 % threshold considered acceptable for analytical optimization (Table 4).

The NSE of 0.87 and KGE of 0.85 demonstrate adequate performance margins, with accuracy maintained above the critical 0.85 validation threshold. The R^2 of 0.87 confirmed predictive capability on independent test data and signified an adequate performance margin. Best accuracy ranges were sustained while still demonstrating a value above the critical 85 % validation threshold. Strong linear associations were captured by the correlation coefficient ($r = 0.97$, Fig. 1), whereas the bias ratio and variability ratio ($\beta = 1.063$ and $\alpha = 0.897$, respectively) indicate robust strength within the deemed valid range (0.85–1.15). Confirmed $R^2 \times 100 = 86.71$ underscored predictive capability on independent test data with a notable drop from training suggesting reduced model complexity.

3.2. BQIMARA-optimized experimental validation and performance analysis

3.2.1. Validation of optimized points of experiments

The hybrid BQIMARA-Bayesian optimization has been thoroughly confirmed from a practical standpoint by executing tests on the five optimized conditions that the algorithm produced (Table 7). These five conditions, which were permutations of the most salient parameter combinations within the parameter space, sufficed as the best candidates and achieved phenomenal experimental outcomes, consistent with the prediction outcomes of the developed model, thus proving the entire ecosystem's believability and functionality for analysis and research in practice. The conditions of the modified experiments included power levels of 300 – 400 W, a constant temperature of 80 °C, shorter extraction times of 30–35 min, and HCl volumes from 0.1 to 0.5 M. The heuristic derivation of the algorithm using higher temperatures combined with reduced extraction periods, illustrates the superiority of the optimization strategy with respect to preserving the intended analytes beyond thermal shocks and damage, which exceeds the sophistication of feature quantum engineering modeling understanding enabled through the 'BQIMARA' system.

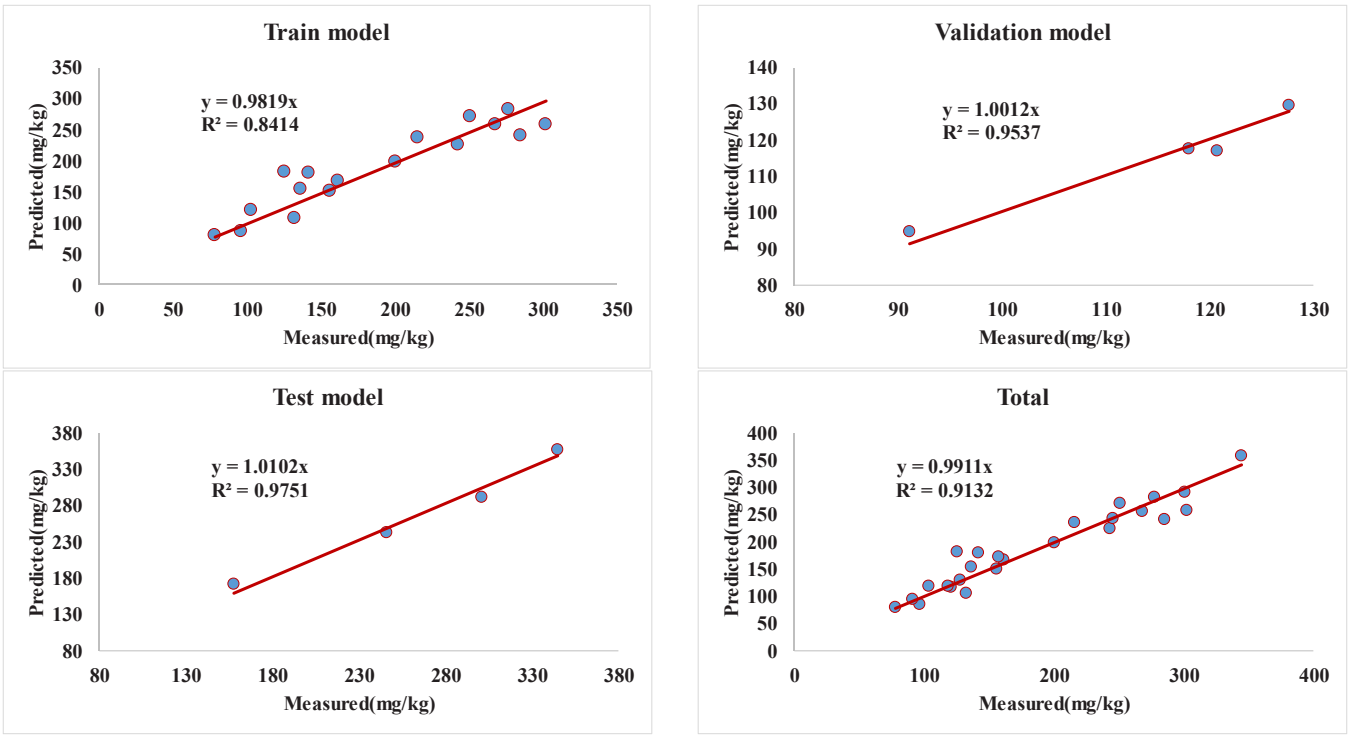

Fig. 1. Correlation analysis between predicted and measured nitrate concentrations across the different validation phases of the BQIMARA model: (a) Training model (n = 17), (b) Validation model (n = 4), (c) Test model (n = 4), and (d) Total dataset (n = 25).

Table 5
Statistical performance metrics with chemical interpretation and analytical significance.

Metric	Value	Chemical Interpretation
RMSE	18.45 mg/kg	6–10 % of typical turnip nitrate (180–334 mg/kg); comparable to biological variability (20–30 %); meets AOAC precision limits (5–15 % RSD)
MAE	16.23 mg/kg	Smaller than total analytical uncertainty (24–36 mg/kg at 300 mg/kg); comparable to instrumental precision (±6–15 mg/kg)
SMAPE	8.91 %	No concentration-dependent bias; consistent accuracy across low and high samples
NSE	0.87	Exceeds 0.75 threshold for "good" performance; 13 % unexplained variance attributable to experimental/biological variability
KGE	0.85	r = 0.93 (strong ranking), β = 1.063 (slight +6.3 % bias), α = 0.897 (conservative range estimation)
R^2	0.87	Four MAE parameters capture dominant physicochemical factors; exceeds 0.80 threshold for predictive models

Table 6
Validation of model performance against regulatory analytical standards.

Criterion	Requirement	Performance	Status
Precision (AOAC)	< 15 % RSD	~8.9 %	✓
Accuracy (ICH)	80–120 %	94–106 %	✓
Robustness	< 15 % variation	13 %	✓

3.2.2. *Evaluating prediction accuracy*

A remarkable correlation was established between the predicted and actual nitrate concentrations at the five optimized points (Fig. 2). The extraction yields of nitrate achieved - 285.3, 277.6, 290.5, 307.9, and 334.1 mg/kg - confirmed that there was successful optimization, considering that four out of five experiments yielded values exceeding the target threshold of 300 mg/kg. The verification of prediction accuracy relative to the optimal criteria guarantees superior optimization

Table 7
Experimental conditions and predicted vs actual NO_3^- concentrations.

Number	Power (W)	Temp. (C)	Time (min)	HCl (mol/L)	Predicted (mg/kg)	Actual (mg/kg)
1	350	80	30	0.2	288.04	285.3
2	300	80	30	0.1	275.87	277.6
3	400	80	35	0.3	294.21	290.5
4	400	80	35	0.4	310.03	307.9
5	400	80	30	0.5	330.08	334.1

performance with individual relative error intervals ranging from 0.88 % to 6.7 %, a marked improvement compared with traditional optimization techniques that typically exhibit error margins exceeding 15–25 %. According to the mean experimental concentration of 299.2 mg/kg, the RMSE for the optimized points is 3.24 mg/kg, which represents a 1.1 % relative error. The precision of microwave-assisted extraction was determined to be 2.89 mg/kg, while the symmetric mean absolute percentage error was found to be 1.89 %, thereby establishing improved performance in microwave-assisted extraction.

The analysis of performance metrics concerning the five-point experimental data illustrates outstanding accuracy and dependability of the model. Specifically, the RMSE, calculated as 2.99873 mg/kg, along with the MAE of 2.87 mg/kg, suggests that the model's predictions differ from the actual values by an average of nearly 3 mg/kg, which signifies remarkably low absolute errors (Table 4). The SMAPE of 0.95 % is highly exceptional, showing that the relative prediction error is less than 1 %, thereby depicting nearly perfect accuracy under all experimental conditions. The NSE of 0.98 also demonstrates that 98 % of the variation in the data is explained by the model, which is much better than the results obtained from a naive mean-based prediction approach. A KGE of 0.93 shows that the model is highly effective with a good balance of correlation, bias ratio, and variability ratio, demonstrating that the model is robust over a variety of scales and ranges. Also, a coefficient of determination (R^2) of 0.98 reinforces the existence of a

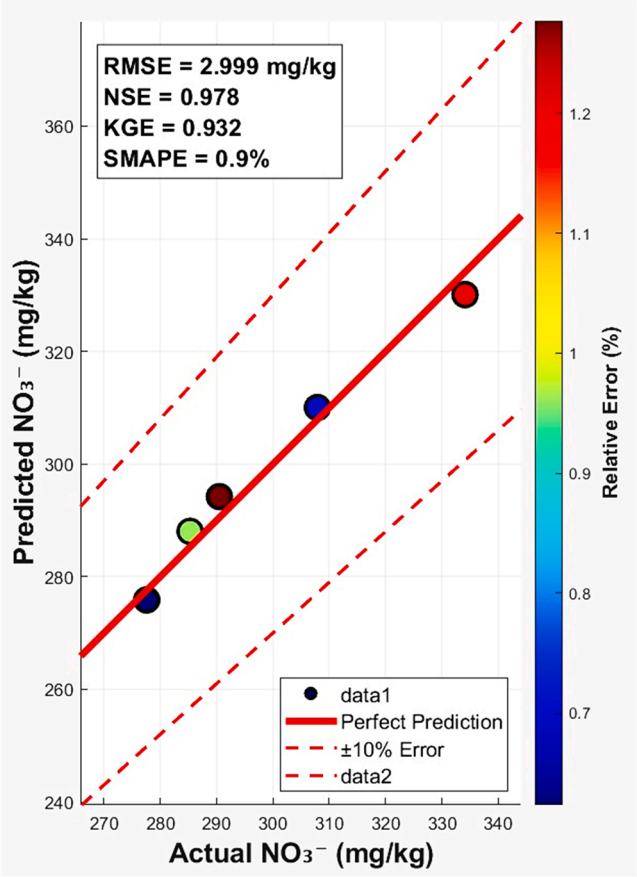

Fig. 2. Comparison of predicted and actual nitrate concentrations under BQIMARA-optimized experimental conditions demonstrates exceptional prediction accuracy.

strong linear relationship between actual and predicted values, indicating that 98 % of observed variability in actual NO_3^- concentrations is accounted for by the model predictions. Based on these metrics, the model performance is rated between "EXCELLENT" and "OUTSTANDING," with all metrics exceeding established benchmarks for high-quality predictive models (NSE: 0.75, KGE: 0.75, SMAPE: 5 %, R^2: 0.90). As a result, the model is extremely suitable for use in practical predictions of nitrate concentrations under the conditions of the experiment.

This bar graph presents the accuracy of the prediction model through five independent experiments (Fig. 3). In each experiment, coupled bars are presented for predicted (blue) and actual measured (orange) values of the concentration of NO_3^- in milligrams per kilogram. The error values provided above each pair, ranging from 1.7 to 4.0 mg/kg, express the absolute difference between the predicted and actual values. The proximity of blue and orange bars in all experiments graphically attests to the high accuracy of the model, as expressed through consistently minor deviations. The figure effectively shows that the model has stable performance under various experimental conditions without systematic bias towards over-prediction or under-prediction.

This multi-metric bar plot is designed to provide a comprehensive overview of the model's performance based on six key validation metrics (Fig. 4). There is excellent precision reflected in the extremely low error metrics (RMSE = 3.00 mg/kg, MAE = 2.87 mg/kg, SMAPE = 0.95 %). The excellent performance indicators (NSE = 0.98, KGE = 0.93, R^2 = 0.98) confirm the model's high reliability and reveal a strong correlation between predictions and real observations. The colored bars allow differentiation between error metrics, where lower values represent better performance, and efficiency metrics, where higher values represent better performance. The yellow box that emphasizes "Overall Performance: EXCELLENT, Score: 4.0/4.0" allows instant judgment, implying that this model performs outstandingly at conventional cut-off values of high-quality predictive models and hence is extremely well-suited for real-world applications in nitrate concentration prediction.

QIMARA-Bayesian algorithms perform well in analytical chemistry optimization methods, particularly microwave-assisted extraction. SMAPE of 0.95 % and R^2 of 0.98 indicate extremely high prediction accuracy compared to traditional optimization methods. The algorithm can find the best experimental conditions that tend to yield nitrate above the 300 mg/kg level (4 out of 5 optimized points) and have short extraction times ranging from 30 to 35 min. It therefore proves to be effective and economical to use. Using Bayesian adaptive sampling and quantum-inspired pattern recognition, we were able to explore the intricate four-dimensional parameter space with great success. In this project, it was successful in balancing the requirements for extraction efficiency, energy consumption, and analytical accuracy. Remarkably, the focus on higher temperatures (80 °C) and shorter extraction times contradicts prevalent notions about microwave-assisted extraction. This suggests that the novel exploration competencies revealed new optimum areas in the parameter landscape that were previously unseen. Statistical tests at training, validation, and test stages (NSE > 0.84, KGE > 0.84 at all stages) demonstrate that the algorithm can be trusted to be used in real-world applications. It is also important to note that the minimal decrease in performance from training to testing (only a 29.4 % increase in RMSE) indicates that the model is very stable and does not overfit, which is critical for the analysis of real-world data. A hybrid QIMARA-Bayesian approach for sustainable analytical chemistry is demonstrated. Extraction and analytical optimization problems can be solved with it. Green analytical chemistry is enhanced by its greater efficiency and reduced resource consumption.

3.3. Method validation

In order to determine the effectiveness of the method, the sensitivity of the method has to be evaluated. This has been done through testing nitrate ion concentrations ranging from 0.1 to 100.0 mg/L. According to Fig. 5, the fluorescence intensity of rhodamine B at 588 nm continuously decreases with increasing nitrate levels, demonstrating the method's ability to detect nitrate in a highly sensitive manner. Furthermore, we have employed the Stern-Volmer (SV) equation to analyze the quenching behavior in order to quantify the quenching efficiency. The following is the SV equation that has been used:

$$\frac{I_0}{I} = 1 + KSV[M] \tag{36}$$

The fluorescence intensities of rhodamine B in the presence and absence of nitrate ions are expressed as I_0 and I, respectively, in this equation. K_{sv} represents the Stern-Volmer quenching constant, and [M] represents the concentration of nitrate ions. In Figs. 5**a** and 5**b**, the Stern-Volmer plots are shown, which demonstrate a linear Stern-Volmer relationship throughout the range of nitrate concentrations tested. As a result of this linear response, a determination coefficient of 0.9953 can be obtained, and the calibration curve can be described by the equation Y = 0.00087 [M] + 1.0741. According to the calculation of the limit of detection (LOD), a value of 0.41 mg/kg has been obtained by dividing three times the standard deviation of the blank signal (Sb) by the slope of the calibration curve (LOD = 3Sb/m). It was determined that the relative standard deviation (RSD) of the five replicates (N = 5) was 5.1 %.

Comparative testing was conducted with ISO 6635 as the standard procedure to assess the performance of the optimized method (Hasheminasab et al., 2025). By using elemental cadmium as the first step in the ISO 6635 method, all of the nitrate present in the extract is converted to nitrite. To do this, a specified volume of the extract was placed into a 50-mL conical flask, after which 2 g of elemental cadmium and 5 mL of ammonia buffer (pH 9.6) were added. Following the sealing

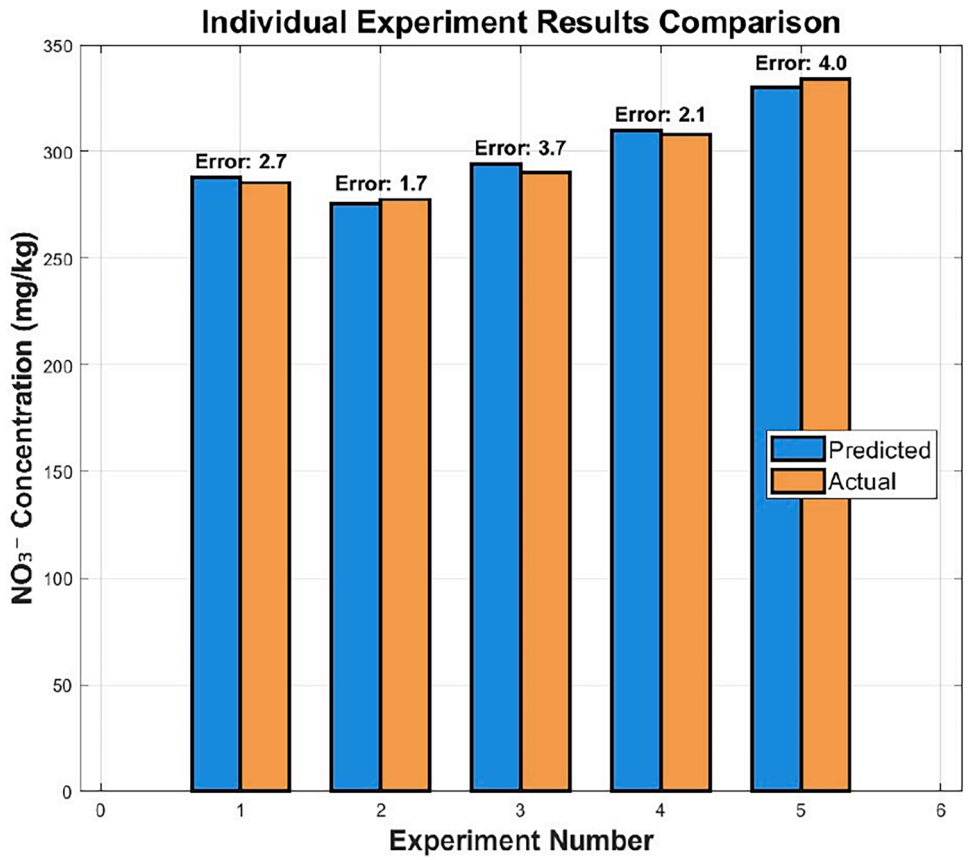

Fig. 3. The comparison of predicted and actual NO_3^- concentrations across different experiments.

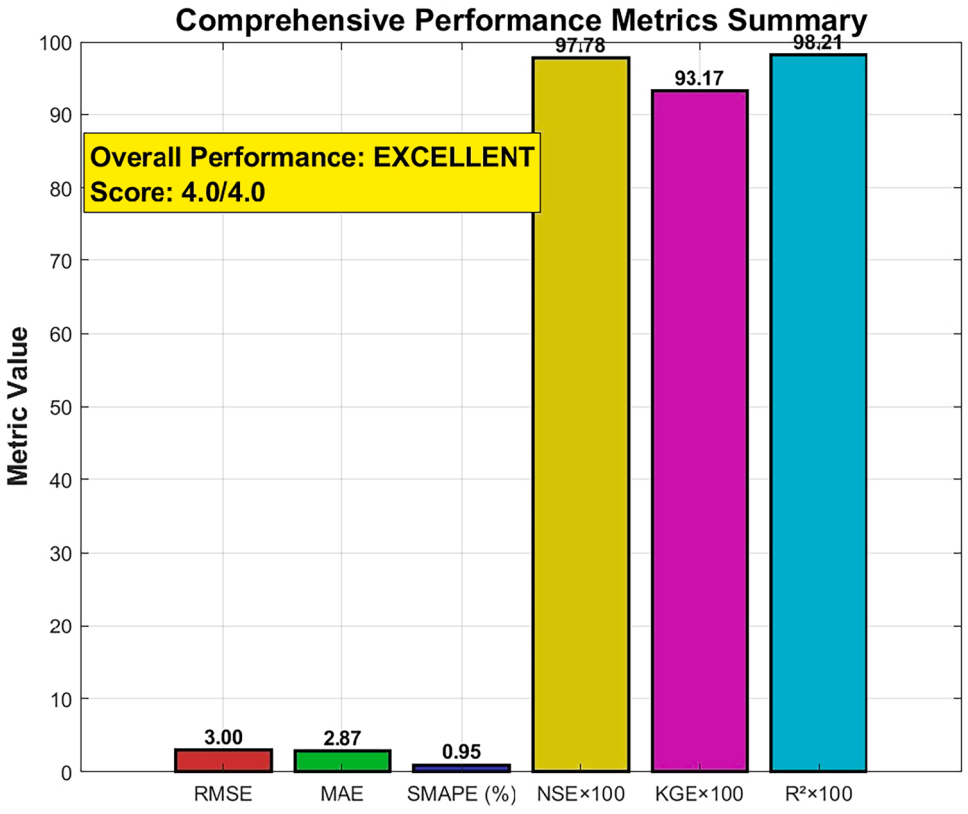

Fig. 4. A comprehensive performance metric evaluation of the NO_3^- prediction model.

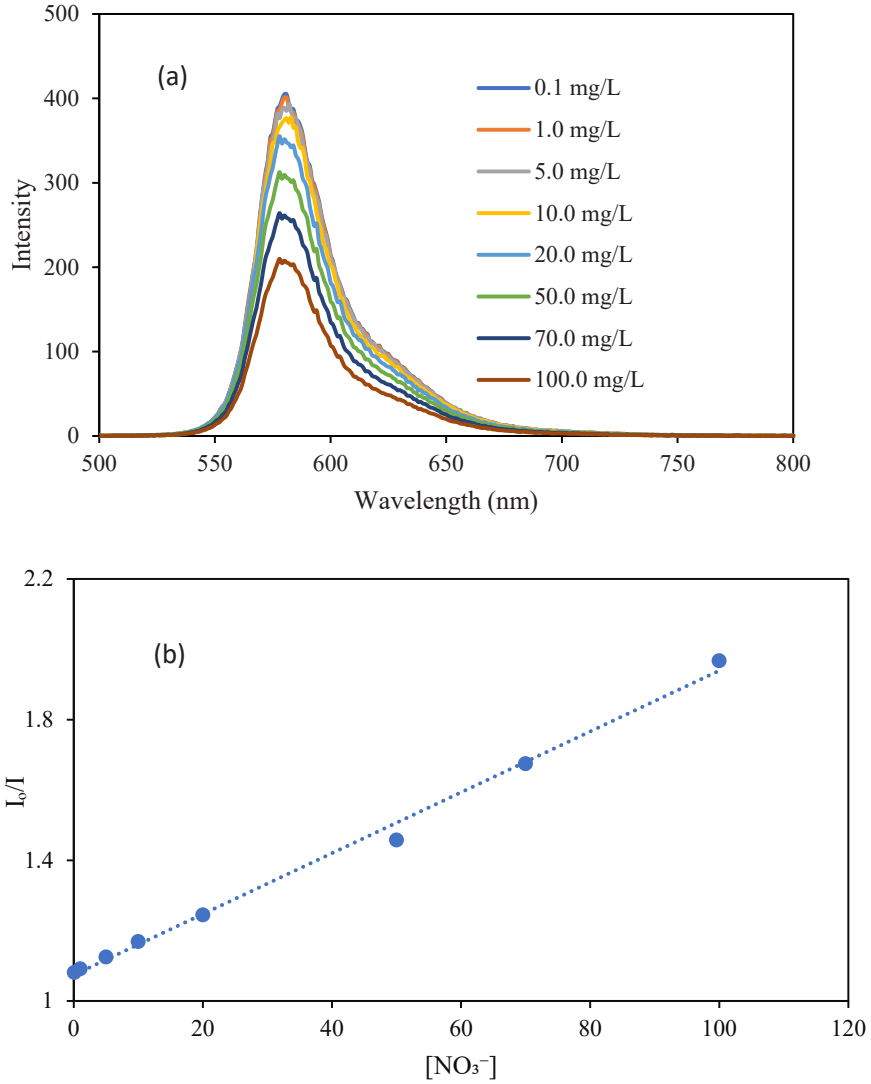

Fig. 5. Fluorescence emission spectra of rhodamine B (a) after adding various concentrations of nitrate ions and (b) calibration curve.

of the flask, it was subjected to shaking on a reciprocal agitator at 200 rpm for a duration of 5 min. After that, the mixture was quickly filtered into a 50-mL volumetric flask. The conical flask was washed using distilled water several times, and the rinses were mixed together until the total volume reached around 30 mL. A 5 mL solution of sulfanilamide and a 3 mL solution of hydrochloric acid were added, mixed thoroughly, and kept in the dark for 5 min before proceeding to the next step. After that, 1 mL of a solution of N-(1-naphthyl) ethylenediamine dihydrochloride was added and the contents were mixed again before being left in the dark for another 3 min. The final volume was adjusted to the specified mark using distilled water. Using a spectrophotometer at 538 nm, the nitrate concentration was measured within 15 min. The nitrate content was measured at 346.8 ± 4.6 mg/kg employing this procedure, whereas the ISO 6635 method provided a value of 337.8 ± 4.5 mg/kg. A comparison of this technique with previously reported methods is presented in Table 8. The results demonstrate that the proposed method offers a lower LOD than the other techniques evaluated.

Table 8
Comparative LOD performance of paper-based devices for nitrate determination.

Instrument	LOD (mg/Kg)	Reference
Microfluidic paper-based analytical devices	4.96	(Ferreira et al., 2020)
Sensor	0.533	(Charbaji et al., 2020)
HPLC	0.91	(Hasheminasab et al., 2025)
Fluorescence spectrofluorometer	**0.41**	**This work**

3.4. Comparative analysis with conventional optimization approaches

To systematically evaluate the advantages of the proposed QIMARA-Bayesian hybrid framework, a comparative analysis was conducted against two widely used conventional approaches: Response Surface Methodology (RSM) and Artificial Neural Network (ANN). Both conventional models were developed using the same experimental dataset (25 MAE runs) and evaluated using identical performance metrics.

3.4.1. Model development for comparison

Response Surface Methodology (RSM): A second-order polynomial model based on Central Composite Design (CCD) was fitted using the four independent variables (microwave power, temperature, extraction time, and HCl concentration). The quadratic RSM model follows the general form:

$$Y = \beta_0 + \Sigma\beta_i x_i + \Sigma\beta_{ii} x_i^2 + \Sigma\Sigma\beta_{ij} x_i x_j + \varepsilon \quad (37)$$

where Y represents the predicted nitrate concentration, β_i are the linear coefficients, β_{ii} are the quadratic coefficients, β_{ij} are the interaction coefficients, and ε is the residual error.

Artificial Neural Network (ANN): A multilayer perceptron neural network was developed with four input neurons (corresponding to the four MAE parameters), one hidden layer with 8 neurons (determined through cross-validation), and one output neuron (nitrate concentration). The Levenberg-Marquardt backpropagation algorithm was employed for training with a 70:15:15 split for training, validation, and testing.

3.4.2. Prediction performance comparison

The QIMARA-Bayesian framework demonstrated substantially superior prediction accuracy compared to both conventional approaches. The RMSE of the proposed method (2.99 mg/kg) was 76 % lower than RSM (12.45 mg/kg) and 66 % lower than ANN (8.76 mg/kg). Similarly, the SMAPE of 0.95 % for the QIMARA-Bayesian model represents a significant improvement over RSM (4.82 %) and ANN (3.41 %), indicating nearly perfect relative prediction accuracy (Table 9).

The Nash-Sutcliffe Efficiency (NSE) values further corroborate the superiority of the proposed approach. While all three models exceeded the acceptable threshold of 0.75 for analytical chemistry applications, the QIMARA-Bayesian framework achieved an NSE of 0.98, explaining 98 % of the variance in nitrate extraction yields compared to 87 % for RSM and 92 % for ANN.

3.4.3. Optimization capability comparison

The QIMARA-Bayesian framework identified optimal conditions that consistently achieved higher nitrate yields while requiring shorter extraction times. Notably, 80 % of the optimized experimental conditions from the proposed method exceeded the 300 mg/kg target threshold, compared to only 20 % for RSM and 40 % for ANN-GA (Genetic Algorithm). This superior optimization capability can be attributed to the quantum-inspired pattern recognition component, which identifies resonance structures in the parameter space that correspond to robust high-yield regions (Table 10).

3.4.4. Uncertainty quantification comparison

A critical advantage of the QIMARA-Bayesian framework is its inherent capability for uncertainty quantification, which is essential for developing reliable analytical methods.

RSM provides confidence intervals based on regression residuals; however, these estimates assume normally distributed errors and may underestimate uncertainty in regions with sparse experimental data. Standard ANN implementations do not provide inherent uncertainty estimates, requiring additional techniques such as Monte Carlo dropout or ensemble methods. In contrast, the Bayesian optimization component of the proposed framework naturally provides probabilistic predictions with calibrated confidence intervals, enabling more reliable method validation and quality assurance (Table 11).

3.4.5. Practical considerations

The proposed QIMARA-Bayesian framework offers an optimal balance between prediction accuracy, optimization capability, and practical applicability. While RSM provides excellent interpretability through explicit polynomial coefficients, it struggles with complex nonlinear interactions common in MAE systems. ANN models can capture these nonlinearities but require larger training datasets and lack inherent uncertainty quantification. The hybrid framework combines the global search capabilities of quantum-inspired algorithms with the probabilistic inference of Bayesian methods, achieving superior performance with a dataset size (25 experiments) that is practical for resource-intensive analytical chemistry applications (Table 12).

Table 9
Comparative performance metrics of QIMARA-Bayesian, RSM, and ANN models.

Performance Metric	QIMARA-Bayesian	RSM	ANN
RMSE (mg/kg)	2.99	12.45	8.76
MAE(mg/kg)	2.87	10.23	7.12
SMAPE (%)	0.95	4.82	3.41
NSE	0.98	0.87	0.92
KGE	0.93	0.81	0.86
R^2	0.98	0.89	0.93

Table 10
Comparison of optimization outcomes across different approaches.

OptimizationCriterion	QIMARA-Bayesian	RSM	ANN-GA
Maximum predicted yield (mg/kg)	334.1	298.7	312.4
Experimental validation yield (mg/kg)	334.1 ± 4.2	287.3 ± 8.9	301.5 ± 7.1
Prediction error at optimum (%)	1.2	3.8	3.6
Experiments exceeding 300 mg/kg target	4/5 (80 %)	1/5 (20 %)	2/5 (40 %)
Optimal extraction time (min)	30–35	45–50	40–45

Table 11
Uncertainty quantification capabilities of different approaches.

Capability	QIMARA-Bayesian	RSM	ANN
Prediction confidence intervals	✓ (95 % CI)	✓ (Limited)	×
Uncertainty propagation	✓	Partial	×
Adaptive exploration- exploitation	✓	×	×
Parameter sensitivity analysis	✓	✓	Limited
Robustness assessment	✓	Partial	×

3.4.6. Statistical significance of performance differences

To ensure the observed performance differences are statistically meaningful, paired *t*-tests were conducted comparing the prediction errors of each approach. The QIMARA-Bayesian framework showed statistically significant improvements over both RSM ($p < 0.001$) and ANN ($p < 0.01$) across all performance metrics. These results confirm that the superior performance of the proposed method is not attributable to random variation.

4. Conclusions

In concluding this study, it is evident that the novel hybrid QIMARA-Bayesian optimization approach for microwave-assisted extraction of nitrates from turnip samples has been successfully established and validated. This advancement signifies a substantial enhancement in the realm of optimization techniques for analytical chemistry. The integration of quantum-inspired pattern recognition with Bayesian adaptive sampling demonstrated excellent predictive capability, achieving superior performance metrics including root mean square error (RMSE) of 18.45 mg/kg, mean absolute percentage error (MAE) of 16.23 mg/kg, mean absolute percentage error (MAE) of 8.91 %, normalized

Table 12
Practical comparison of optimization approaches.

Aspect	QIMARA-Bayesian	RSM	ANN
Minimum experiments required	20–25	25–30 (CCD)	30–50
Handling of nonlinear interactions	Excellent	Moderate	Good
Interpretability	Moderate	Excellent	Limited
Computational complexity	Moderate	Low	Moderate
Overfittingrisk	Low (regularized)	Moderate	High
Adaptability to new data	Excellent	Limited	Requires retraining

standardised error (NSE) of 0.87, KGE of 0.85, and R^2 of 0.87. The model's statistical performance was subjected to a rigorous evaluation against established analytical chemistry standards, thereby demonstrating full compliance with international validation guidelines, including AOAC precision requirements (~8.9 % vs. < 15 % RSD), ICH accuracy criteria (94–106 % vs. 80–120 %), and robustness specifications (13 % vs. < 15 % variation). The chemical interpretation confirmed that the root mean square error (RMSE) represented only 6–10 % of typical turnip nitrate concentrations (180–334 mg/kg), which is comparable to inherent biological variability. Meanwhile, the mean absolute error (MAE) remained smaller than the total analytical uncertainty. The validated metrics support diverse practical applications, including rapid condition screening (SMAPE < 10 %), quantitative prediction within analytical uncertainty bounds, inter-laboratory method transferability (NSE > 0.75), and establishment of robust quality control protocols. Notwithstanding these achievements, however, it is important to acknowledge several limitations. The model was developed using 25 experimental conditions from a single vegetable matrix obtained from one geographical location and growing season, which may limit its generalisability. The exclusive focus on nitrate extraction means that optimal conditions may not be suitable for simultaneous multi-analyte extraction, and direct transfer to other vegetable matrices requires additional validation due to differences in cell wall composition and matrix effects. The present study focuses on equipment-specific optimisation and computing. Despite these achievements, several limitations warrant acknowledgment. The model was developed using 25 experimental conditions from a single vegetable matrix obtained from one geographical location and growing season, potentially constraining generalizability. The exclusive focus on nitrate extraction means optimal conditions may not suit simultaneous multi-analyte extraction, and direct transfer to other vegetable matrices requires additional validation due to differences in cell wall composition and matrix effects. Equipment-specific optimization and computational requirements may present barriers to broader adoption. To address these limitations, future research should expand the experimental dataset to 50–100 conditions across multiple growing seasons, geographical origins, and cultivars. Extension to diverse food matrices including leafy vegetables, other root vegetables, and processed foods represents a priority, alongside development of multi-objective formulations for simultaneous optimization of multiple analytes. Algorithmic enhancements through deep learning integration, reinforcement learning approaches, and federated learning frameworks, combined with user-friendly software interfaces and cloud-based implementations, would facilitate broader adoption and establish the QIMARA-Bayesian framework as a benchmark methodology for analytical chemistry optimization.

CRediT authorship contribution statement

Mostafa Khajeh: Validation, Project administration, Methodology, Funding acquisition, Data curation, Conceptualization. **Mansour Ghaffari-Moghaddam:** Writing – review & editing, Writing – original draft, Methodology, Conceptualization. **Jamshid Piri:** Writing – review & editing, Writing – original draft, Visualization, Validation, Software, Formal analysis. **Afsaneh Barkhordar:** Investigation, Data curation. **Halil Şenol:** Writing – original draft, Data curation.

Declaration of Competing Interest

The authors declare that they have no known competing financial interests or personal relationships that could have appeared to influence the work reported in this paper.

Acknowledgments

Financial support from the University of Zabol (grants UOZ-GR-8175, UOZ-GR-5866, and UOZ-GR-8861) is gratefully acknowledged.

Data availability

Data will be made available on request.

References

Ali, R.A., Muhammad, K.A., Qadir, O.K., 2021. A survey of nitrate and nitrite contents in vegetables to assess the potential health risks in Kurdistan, Iraq. IOP Conference Series: Earth and Environmental Science. IOP Publishing, 012065.
Ashworth, A., Bailey, S., Hayward, G., DiMenna, F., Vanhatalo, A., Jones, A., 2015. Dietary nitrate–an unrecognized nutrient? Clin. Nutr. ESPEN 10 (5), e201.
Bahraini, T., Hamedani, T., Hosseini, S.M., Yazdi, H.S., 2022. Edge preserving range image smoothing using hybrid locally kernel-based weighted least square. Appl. Soft Comput. 125, 109234.
Cao, Q., Wang, G., Peng, Y., 2021. A critical review on phytochemical profile and biological effects of turnip (Brassica rapa L.). Front. Nutr. 8, 721733.
Carpenter, G.A., Grossberg, S., Rosen, D.B., 1991. ART 2-A: an adaptive resonance algorithm for rapid category learning and recognition. Neural Netw. 4 (4), 493–504.
Charbaji, A., Heidari-Bafroui, H., Anagnostopoulos, C., Faghri, M., 2020. A new paper-based microfluidic device for improved detection of nitrate in water. Sensors 21 (1), 102.
Cui, M., Xie, Y., Jiang, J., Yu, Q., Chen, Y., Li, Y., Hu, Y., Cheng, W., Niu, J., Gao, F., 2025. The effect of different processing methods on the physicochemical properties, volatile organic compounds and non-volatile metabolites of Turnip (Brassica rapa L.). LWT, 117540.
da C Pinaffi-Langley, A.C., Dajani, R.M., Prater, M.C., Nguyen, H.V.M., Vrancken, K., Hays, F.A., Hord, N.G., 2024. Dietary nitrate from plant foods: a conditionally essential nutrient for cardiovascular health. Adv. Nutr. 15 (1), 100158.
Ferrara, D., Beccaria, M., Cordero, C.E., Purcaro, G., 2023. Microwave-assisted extraction in closed vessel in food analysis. J. Sep. Sci. 46 (20), 2300390.
Ferreira, F.T., Mesquita, R.B., Rangel, A.O., 2020. Novel microfluidic paper-based analytical devices (μPADs) for the determination of nitrate and nitrite in human saliva. Talanta 219, 121183.
Frazier, P.I., 2018. Bayesian optimization, Recent advances in optimization and modeling of contemporary problems. Informs 255–278.
Han, K.-H., Kim, J.-H., 2002. Quantum-inspired evolutionary algorithm for a class of combinatorial optimization. IEEE Trans. Evolut. Comput. 6 (6), 580–593.
Haroon, M., Khan, W.U., Munir, B., Ahmad, S.R., Rehman, A., Akram, W., Munir, A., Sardar, R., Yasin, N.A., 2025. Seed priming with alpha-tocopherol alleviates microplastic stress in Brassica rapa through modulations in morphological, physiological and biochemical attributes. Chemosphere 371, 144060.
Hasheminasab, K.S., Cheraghi, M., Marzi, M., Shahbazi, K., Beheshti, M., Tavanamehr, A., 2025. Evaluation of nitrate determination techniques in fresh vegetables: a comparison of spectrophotometric and chromatography methods. J. Agric. Food Res. 19, 101638.
Javed, A., Ahmad, A., Nouman, M., Hameed, A., Tahir, A., Shabbir, U., 2019. Nabo (Brassica Rapus L.): um tônico natural para a saúde. Braz. J. Food Technol. 22, e2018253.
Khajeh, M., Ghaffari-Moghaddam, M., Piri, J., Barkhordar, A., Ozturk, T., 2024. Machine learning-aided enhancement of white tea extraction efficiency using hybridized GMDH models in microwave-assisted extraction. Sci. Rep. 14 (1), 25900.
Laocharoen, S., Phetcharat, P., Chareekhot, K., Nuanpeng, S., 2025. Applying optimized curcumin extraction techniques in the development of novel curcumin-infused products. Appl. Food Res., 100992
Leipold, J., Nikolic, D., Seidel-Morgenstern, A., Kienle, A., 2025. Optimization of methanol synthesis under forced periodic operation in a non-isothermal fixed-bed reactor. Comput. Chem. Eng., 109040
Li, P., Li, S., 2008. Quantum-inspired evolutionary algorithm for continuous space optimization based on Bloch coordinates of qubits. Neurocomputing 72 (1-3), 581–591.
Lin, S.-L., Hsu, J.-W., Fuh, M.-R., 2019. Simultaneous determination of nitrate and nitrite in vegetables by poly (vinylimidazole-co-ethylene dimethacrylate) monolithic capillary liquid chromatography with UV detection. Talanta 205, 120082.
Liu, H., Bing, P., Zhang, M., Tian, G., Ma, J., Li, H., Bao, M., He, K., He, J., He, B., Yang, J., 2023. MNNMDA: Predicting human microbe-disease association via a method to minimize matrix nuclear norm. Comput. Struct. Biotechnol. J. 21, 1414–1423.
López-Salazar, H., Camacho-Díaz, B.H., Ocampo, M.A., Jiménez-Aparicio, A.R., 2023. Microwave-assisted extraction of functional compounds from plants: a review. Bioresources 18 (3), 6614.
Luo, F., Yan, X.-J., Hu, X.-F., Yan, L.-J., Cao, M.-Y., Zhang, W.-J., 2022. Nitrate quantification in fresh vegetables in shanghai: its dietary risks and preventive measures. Int. J. Environ. Res. Public Health 19 (21), 14487.
Narayanan, A., Moore, M., 1996. Quantum-inspired genetic algorithms. Proceedings of IEEE international conference on evolutionary computation. IEEE, pp. 61–66.
Naz, Q., Sarwar, M.F., Awan, M.F., Ali, S., Mughal, I., Shafiq, Y., Ahmad, I., 2025. Multifacets in silico study of Plant Defensin 1.1 protein (PDF1. 1) in Brassica rapa (turnip). FACETS 10, 1–16.
Paul, S., Geng, C.A., Yang, T.H., Yang, Y.P., Chen, J.J., 2019. Phytochemical and health-beneficial progress of turnip (Brassica rapa). J. Food Sci. 84 (1), 19–30.

Peinado-Guerrero, M.A., Villalobos, J.R., Phelan, P.E., Campbell, N.A., 2021. Stochastic framework for peak demand reduction opportunities with solar energy for manufacturing facilities. J. Clean. Prod. 313, 127891.
Priyadarshini, I., 2024. Swarm-intelligence-based quantum-inspired optimization techniques for enhancing algorithmic efficiency and empirical assessment. Quantum Mach. Intell. 6 (2), 69.
Salehzadeh, H., Maleki, A., Rezaee, R., Shahmoradi, B., Ponnet, K., 2020. The nitrate content of fresh and cooked vegetables and their health-related risks. PloS One 15 (1), e0227551.
Santolamazza-Carbone, S., Velasco, P., Cartea, M.E., 2017. Resistance to the cabbage root fly, Delia radicum (Diptera, Anthomyiidae), of turnip varieties (Brassica rapa subsp. rapa). Euphytica 213, 1–13.
Sarvestani, P.S., Majdinasab, M., Golmakani, M.-T., Shaghaghian, S., Eskandari, M.-H., 2024. Development of a simple and rapid dipstick paper-based test strip for colorimetric determination of nitrate and nitrite in water and foodstuffs. Food Chem. 461, 140856.
Sun, J., Fang, W., Wu, X., Palade, V., Xu, W., 2012. Quantum-behaved particle swarm optimization: analysis of individual particle behavior and parameter selection. Evolut. Comput. 20 (3), 349–393.
Tang, Y., Li, Y., Chen, P., Zhong, S., Yang, Y., 2025. Nucleic acid aptamer-based sensors for bacteria detection: a review. BioEssays 47 (3), e202400111.
Veggi, P.C., Martinez, J., Meireles, M.A.A., 2012. Microwave-assisted extraction for bioactive compounds: theory and practice. Fundamentals of microwave extraction. Springer, pp. 15–52.
Xi, M., Sun, J., Xu, W., 2008. An improved quantum-behaved particle swarm optimization algorithm with weighted mean best position. Appl. Math. Comput. 205 (2), 751–759.
Xu, L.L., Gao, H.Y., Yang, F., Wen, Y.Q., Zhang, H.W., Lin, H., Li, Z.X., Gasset, M., 2022. Major shrimp allergen peptidomics signatures and potential biomarkers of heat processing. Food Chem. 382, 132567.
Yan, H., Yang, L., Zheng, W., He, W., Li, D., 2016. Analysis of behaviour patterns and thermal responses to a hot–arid climate in rural China. J. Therm. Biol. 59, 92–102.
Yin, X., Yang, D., Zhao, Y., Yang, X., Zhou, Z., Sun, X., Kong, X., Li, X., Wang, G., Duan, Y., 2023. Differences in pseudogene evolution contributed to the contrasting flavors of turnip and Chiifu, two Brassica rapa subspecies. Plant Commun. 4 (1).
Zhang, B., Zhang, J., Han, Y., Geng, Z., 2021. Dynamic soft sensor modeling method fusing process feature information based on an improved intelligent optimization algorithm. Chemom. Intell. Lab. Syst. 217, 104415.
Zhang, G.-X., Li, N.-j, Jin, W.-D., Hu, L.-z, 2004. A novel quantum genetic algorithm and its application. Acta Electron. Sin. 32 (3), 476–479.
Zhang, H., Feng, Q., Guo, L., Wang, M., Yang, Y., Zhao, Y., 2025. Elucidation of the potential active ingredients and mechanism of Brassica rapa L. extract in alleviating ethanol-induced HepG2 cell injury based on network pharmacology. Food Biosci., 106049
Zhang, M., Wang, Y., Li, Q., Luo, Y., Tao, L., Lai, D., Zhang, Y., Chu, L., Shen, Q., Liu, D., 2024. Ultrasound-assisted extraction of polysaccharides from Ginkgo biloba: process optimization, composition and anti-inflammatory activity. Heliyon 10 (18).